

# Remote Sensing Drought Indices for the Semi-Arid Region of Southeast Brazil

Antônio H. de C. Teixeira<sup>1</sup>, Janice F. Leivas<sup>2</sup>, Fulvio R. Simão<sup>3</sup>, and João B. R. S. Reis<sup>3</sup>

1. Embrapa Coastal Tablelands, Brazil

2. Embrapa Satellite Monitoring, Brazil

3. Minas Gerais Agricultural Research Institute, Brazil

**Abstract:** The semi-arid region of the Minas Gerais state, Southeast Brazil, has experienced some events of drought, while arising large irrigation schemes in some areas increasing water withdrawn from the rivers. These scenarios demand large-scale water balance studies to subsidize water resources policies. The visible, infrared and thermal bands from Landsat 8 satellite images were used together with a net of agrometeorological stations to test drought indices in this region, during the year 2015, classifying irrigated areas and natural vegetation, aiming mitigations for climatically water scarcity. The  $ET_r$  index (i.e., the ratio of actual – ET to reference –  $ET_0$  evapotranspiration) was obtained by using the SAFER (Simple Algorithm for Evapotranspiration Retrieving) algorithm, while the SUREAL (Surface Resistance Algorithm) algorithm was applied to estimate the surface resistance to water vapor transfer ( $r_s$ ). The highest and lowest  $ET_r$  and  $r_s$  values, meaning better root-zone moisture conditions, above 0.90 and bellow 800  $s m^{-1}$ , respectively, happened in the counties with the largest concentrations of irrigation area, resulting in an increment on ET of 3.0  $mm d^{-1}$ , because of the replacement of natural vegetation by irrigated crops. On the other hand, outside the rainy period, natural vegetation showed  $ET_r$  values close to 0.00 and  $r_s$  very high, above 1000  $s m^{-1}$ . Between the two drought indices,  $r_s$  detected better the different soil moisture conditions. The results are relevant for monitoring drought events under the additional environmental consequences of land use change in semi-arid environments.

**Key words:** evapotranspiration, soil moisture, water resources

## 1. Introduction

Drought events can occur in any agro-ecosystems, from a range of hydrometeorological processes that suppress precipitation and/or limit the root-zone water availability, creating conditions that are significantly drier than normal or otherwise limiting moisture availability to a potentially damaging extent. Agrometeorological indices may be used to help track drought events, depending on the spatial and time scale [1].

Drought impacts are significant and widespread in many hydrological basins, increasing disputes over

their water resources. Under these conditions, more conflicts are expected as populations expand, economies grow, and the competition for the scarce water supplies during these drier events intensifies [2].

Aiming a sustainable exploration of the water resources, water managers should consider the large-scale water balance conditions of the mixed agro-ecosystems in the hydrological basins, to subsidize policies that minimizes the water use by agriculture while maintaining the water availability [3].

Drought events can adversely affect agriculture and food security and their impacts can vary by region and by season. Agriculture in the North of Minas Gerais state, Southwest Brazil, has been highlighted by increasing water demands for irrigation, with fast replacement of natural vegetation by irrigated crops.

**Corresponding author:** Antônio Heriberto de Castro Teixeira, Ph.D.; research areas/interests: agrometeorology, environmental sciences, remote sensing. E-mail: heriberto.teixeira@embrapa.br.

On the one hand, the largest part of the agricultural products in the North of Minas Gerais are for the external markets. On the other hand, the main impact between the use of the water resources and the environment is large water withdrawn from the rivers, reducing their flow to the ocean, and the pollution caused by the agricultural drainage, which is becoming worse together with several drought events during the recent years [4].

For analyzing drought events, besides rainfall, it is also important to quantify the water fluxes from the vegetated surface to the lower atmosphere. Considering the indices used in the current paper, it is important to point out the distinctions between reference ( $ET_0$ ) and actual (ET) evapotranspiration. The first agrometeorological parameter is considered as the water flux from a reference surface as grass, with specific characteristics, while the second one is the real water flux involving all environmental conditions [5].

In well-irrigated crops, the values of the drought index taken here, the evapotranspiration ratio —  $ET_r$  ( $ET/ET_0$ ) are known as the crop coefficient —  $K_c$ , used to estimate the water requirements from vegetated surfaces [5], while in natural vegetation,  $ET_r$  can characterize the water stress conditions [6]. Regarding the drought index also considered, the surface resistance to water fluxes ( $r_s$ ), as lower are its values, as higher are the root-zone moistures, for all kind of vegetation [7].

Under favorable conditions for irrigation, agriculture in the semi-arid region of the North of Minas Gerais state, Southeast Brazil, has been growing. Under these circumstances, application of large-scale drought indices can subsidize monitoring water and vegetation conditions [1].

The objective of this paper was to combine geo technologies for modelling large-scale drought indices throughout the joint use of satellite images and agrometeorological data in semi-arid region of the North of Minas Gerais state, Southeast Brazil, during the year 2015. The SAFER (Simple Algorithm for

Evapotranspiration Retrieving) algorithm is used to estimate large-scale  $ET_r$  and ET values, while to classify the agro-ecosystems into irrigated crops (IC) and natural vegetation (NV) the SUREAL (Surface Resistance Algorithm) algorithm is applied considering  $r_s$  threshold values. The results may be used for drought risk management aiming mitigation policies to minimize water scarcity problems.

## 2. Material and Methods

A net of twelve agrometeorological stations and four Landsat 8 satellite images involving different thermohydrological conditions along the year 2015 were used together with the SAFER and the SUREAL algorithms in the North of Minas Gerais state, Southeast Brazil.

Fig. 1 shows the location of the study region, with the County divisions and the agrometeorological stations: Mocambinho (MC), Matias Cardoso (MC), Gameleiras (GA), Jaíba (JB), Varzelândia (VZ), Pai Pedro (PP), Nova Porteirinha (NP), São João da Ponte (SJP), Riacho dos Machados (RM), Bela Vista (BV) and Capitão Eneas (CE).

The agrometeorological stations are composed of sensors to obtain the global incident radiation ( $R_G$ ); air temperature ( $T_a$ ); relative air humidity (RH); wind speed at a height of 2 m (u); and precipitation (P).

These agrometeorological variables allowed the calculation of  $ET_0$ , by the Penman-Monteith method [5], representing the atmosphere demand and the input of natural water to the mixed agro-ecosystems.

The weather data were interpolated by the moving average method generating grids with pixel size of 30 m, compatible to the spatial resolution of the visible and infrared bands of the Landsat 8 images.

The native vegetation types in the semi-arid region of the study region are classified as “Cerrado”, “Caatinga” and transitions between these ecosystems. However, nowadays, irrigated crops, mainly fruits and grains, are replacing the natural species.

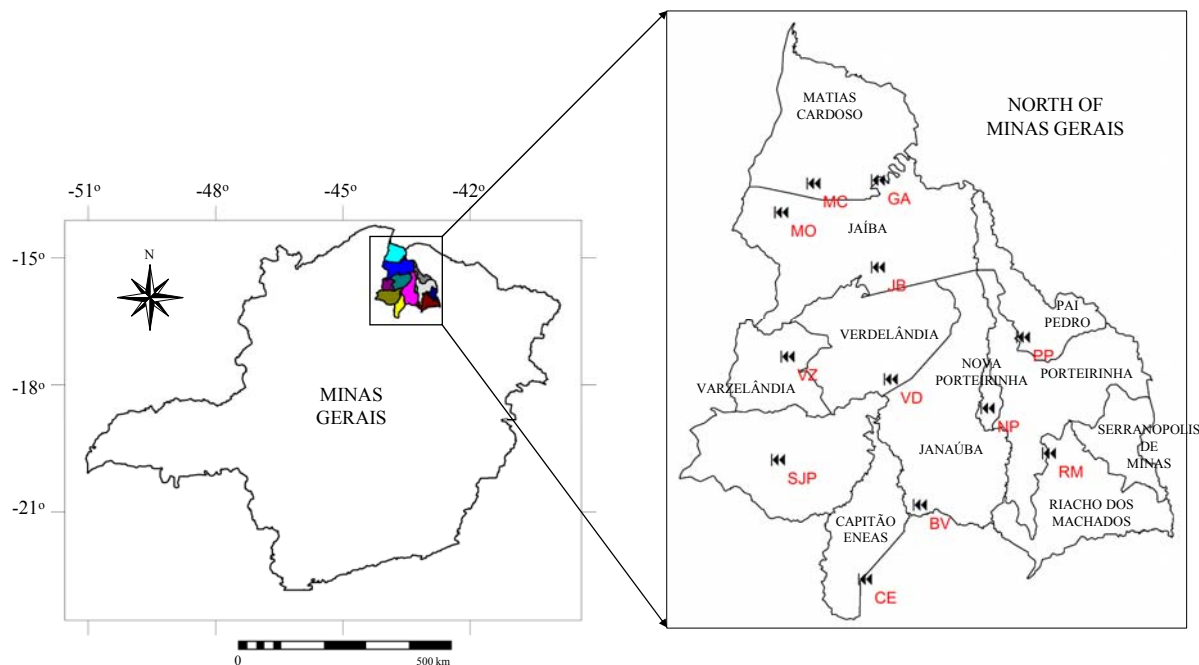


**Fig. 1** Location of the agrometeorological stations inside the counties under the semiarid conditions of the Minas Gerais state, Southeast Brazil.

According to Lumbreiras et al. [9], the long-term annual total of precipitation ( $P$ ) is below  $900 \text{ mm yr}^{-1}$ , with the rains concentrated in the first and the last quarters of the year. The thermal conditions are characterized by high air temperatures ( $T_a$ ), typically of tropical climates, with long-term daily average of  $24^\circ\text{C}$  and maximum and minimum of  $32^\circ\text{C}$  and  $14^\circ\text{C}$ , respectively in October and July.

The Landsat 8 images used were from the orbit 218, points 70 and 71, from which mosaics involved different thermohydrological conditions along the year 2015, presented in terms of day of the year (DOY), January 19 (DOY 019), June 12 (DOY 163), September 16 (DOY 259) and November 03 (DOY 307).

Fig. 2 shows the flowchart for the large-scale drought indices modelling by using Landsat 8 images together with agrometeorological data throughout the SAFER and SUREAL algorithms. The bands 1 to 7 (spatial resolution of  $30 \text{ m}$ ) were used to calculate the surface albedo ( $\alpha_0$ ) and the Normalized Difference Vegetation Index (NDVI), while for the surface temperature ( $T_0$ ), this was done with the bands 10 and

11 (spatial resolution of  $100 \text{ m}$ ).

All the regression coefficients of the equations for acquiring the parameters in Fig. 2 were determined in the semi-arid area showed of Northeast Brazil with simultaneous Landsat satellite and field measurements, involving strongly contrasting agro-ecosystems and under different thermohydrological conditions throughout different years [10].

Following Fig. 2, according to Teixeira et al. [8], the spectral radiances ( $L_\lambda$ ) were computed from Digital Numbers (DN):

$$L_\lambda = aDN + b \quad (1)$$

where  $a$  and  $b$  are regression coefficients given in the metadata file [11].

The planetary albedo for each Landsat satellite band ( $\alpha p_\lambda$ ) was calculated as:

$$\alpha p_\lambda = \frac{L_\lambda \pi d^2}{R_{\lambda} \cos \varphi} \quad (2)$$

where  $L_\lambda$  is the spectral radiance for a band ( $\text{W m}^{-2} \text{ sr}^{-1} \mu\text{m}^{-1}$ ),  $d$  is the relative earth-sun distance;  $R_{\lambda}$  is the

mean solar irradiance at the top of the atmosphere for

each band ( $\text{W m}^{-2} \mu\text{m}^{-1}$ ) and  $\phi$  the solar zenith angle.

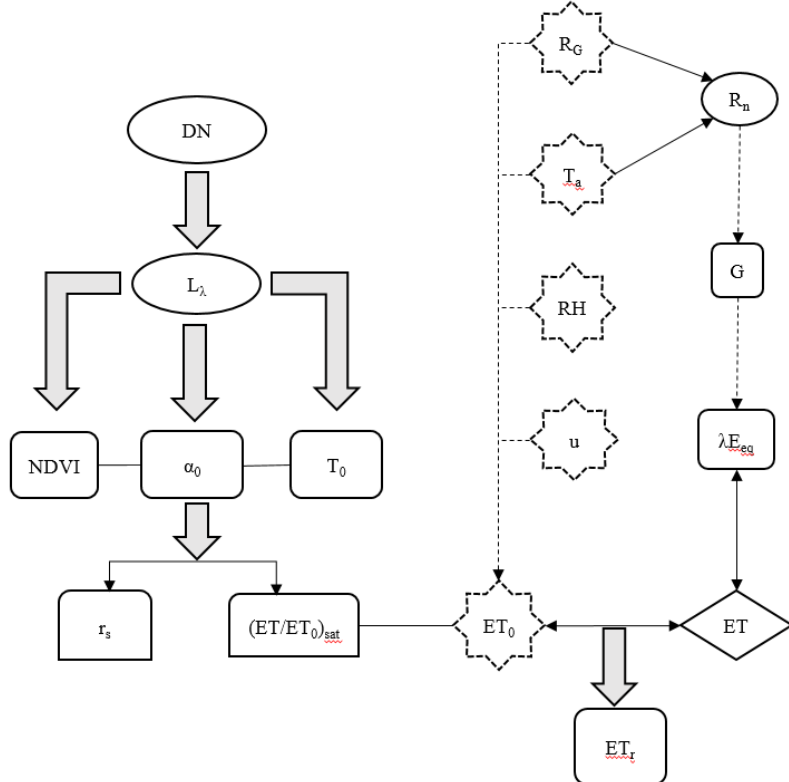


**Fig. 2** Flowchart for modeling the drought indices with Landsat 8 images, throughout application of the SAFER (Simple Algorithm for Evapotranspiration Retrieving), SUREAL (Surface Resistance Algorithm) algorithm, and interpolated agrometeorological data.

The broadband planetary albedo ( $\alpha_p$ ) was calculated as the total sum of the different narrow-band  $\alpha p_\lambda$  values according to the weights for each band ( $w_\lambda$ ).

$$\alpha p = \sum w_\lambda \alpha p_\lambda \quad (3)$$

The spectral radiances from the bands 10 and 11 from the Landsat 8 thermal regions at the top of the atmosphere ( $T_\lambda$ ) were obtained by inversion of the Plank's law in the 10.6-11.19  $\mu\text{m}$  (band 10) and 11.5-12.51  $\mu\text{m}$  (band 11) bandwidth:

$$T_\lambda = \frac{K_2}{\ln(\frac{K_1}{L_\lambda + 1})} \quad (4)$$

where  $K_1$  (774.89 and 480.89) and  $K_2$  (1321.08 and 1201.14) for bands 10 and 11, respectively, are conversion coefficients. The average  $T_\lambda$  value from the two bands was considered as the brightness temperature ( $T_{\text{bright}}$ ).

Both  $\alpha_p$  and  $T_{bright}$  were corrected atmospherically for acquiring the albedo ( $\alpha_0$ ) and temperature ( $T_0$ ) surface values, by regression equations determined by previous simultaneous Landsat and field measurements.

The daily values for net radiation ( $R_n$ ) were estimated by using the Slob equation, with data on  $R_G$  and  $T_a$ :

$$R_n = (1 - \alpha_0) R_G - a_L \tau_{sw} \quad (5)$$

where  $\tau_{sw}$  is the atmospheric transmissivity calculated as the ratio of  $R_G$  to the incident solar radiation at the top of the atmosphere ( $R_a$ ) and the regression coefficient  $a_L$  was spatially distributed through its relationship with  $T_a$ .

The SAFER algorithm is used to model the ratio of the actual to the reference evapotranspiration based on the input remote sensing parameters at the satellite

overpass time ( $ET/ET_0$ )<sub>sat</sub>, which is then multiplied by  $ET_0$  24-hour grids to estimate the daily large-scale ET values:

$$\left( \frac{ET}{ET_0} \right)_{sat} = \exp \left[ a_{sf} + b_{sf} \left( \frac{T_0}{\alpha_0 NDVI} \right) \right] \quad (6)$$

where  $a_{sf}$  and  $b_{sf}$  are the original regressions coefficients, 1.8 and -0.008, respectively [10].

Eq. (6) does not work for water bodies, i.e. when  $NDVI < 0$ . Thus, as in the study region, sometimes some areas are mixtures of land and water, in the SAFER algorithm the equilibrium (subscript *eq*) evapotranspiration [12] is considered under these conditions, and the latent heat flux ( $\lambda E_{eq}$ ) retrieved throughout conditional functions and transformed into  $ET_{eq}$ :

$$\lambda E_{eq} = \frac{s(R_n - G)}{s + \gamma} \quad (7)$$

where  $s$  is the slope of the curve relating saturation water vapor pressure to  $T_a$ ,  $G$  is the ground heat flux considered as fraction of  $R_n$  and  $\gamma$  is the psychometric constant.

After considering the results for ET taking into account both Eqs. (6) and (7) by applying conditional

functions to the NDVI pixel values, a drought indicator, related to soil moisture conditions, the evapotranspiration ratio ( $ET_r$ ) was used:

$$ET_r = \frac{ET}{ET_0} \quad (8)$$

High  $ET_r$  values indicate that vegetation are well supplied with water, while low values mean root-zone water stress.

By applying the SUREAL algorithm, another large-scale drought index was used; the surface resistance to water fluxes ( $r_s$ ) [7]:

$$r_s = \exp \left[ a_r \left( \frac{T_0}{\alpha_0} \right) (1 - NDVI) + b_r \right] \quad (9)$$

where  $a_r$  and  $b_r$  are regression coefficients

### 3. Results and Discussion

Fig. 3 presents the tendencies of the fortnightly values for the mean totals of precipitation (P) and  $ET_0$  pixels in terms of day of the year (DOY), inside the study area covering the counties showed in Fig. 1. The period embraces conditions previous, during and after the image acquisitions from 2014 to 2015.

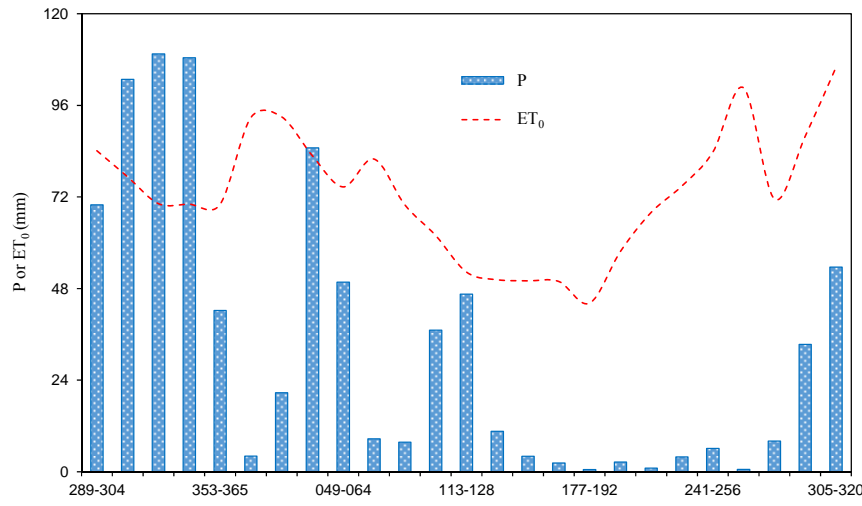


**Fig. 3** Climatic water balance in the North of Minas Gerais state, Southeast Brazil, embracing the fortnightly periods from 2014 to 2015, previous, during and after the image acquisitions, precipitation (P) and reference evapotranspiration ( $ET_0$ ).

Due the semi-arid characteristics of the study region, P was much more changeable than  $ET_0$ . For the whole

period depicted in Fig. 3, rainfalls concentrated at the end of 2014 and at the start of 2015. The driest

conditions, with P dropping to around 5 mm, were from DOY 160 to 289 in 2015, bellow than 10% of the  $ET_0$  values. However, one can see dry spells in January from DOY 064 to 097, during the rainy season of 2015, with P corresponding to only 4% of  $ET_0$ , what coupled with high atmospheric demand, contributed for a drought event.

The largest  $ET_0$  values happened at the start and at the end of the year 2015, with pixel averages above 5.5  $\text{mm d}^{-1}$ .

Increasing P and  $ET_0$  values during the first half of the year 2015 were in favor for the highest both, ET

and biomass production (BIO) for the NV and IC agro-ecosystems. However, in the second half of the year, under low rainfall amounts, only IC was favored for high ET and BIO rates, resulting in strong hydrological contrast when comparing with the NV ecosystem, constituted mainly by the “Caatinga” species.

Fig. 4 shows the spatial distribution and average daily  $ET_r$  values, for different thermohydrological conditions of the year 2015, in the North of Minas Gerais state, Southeast Brazil.

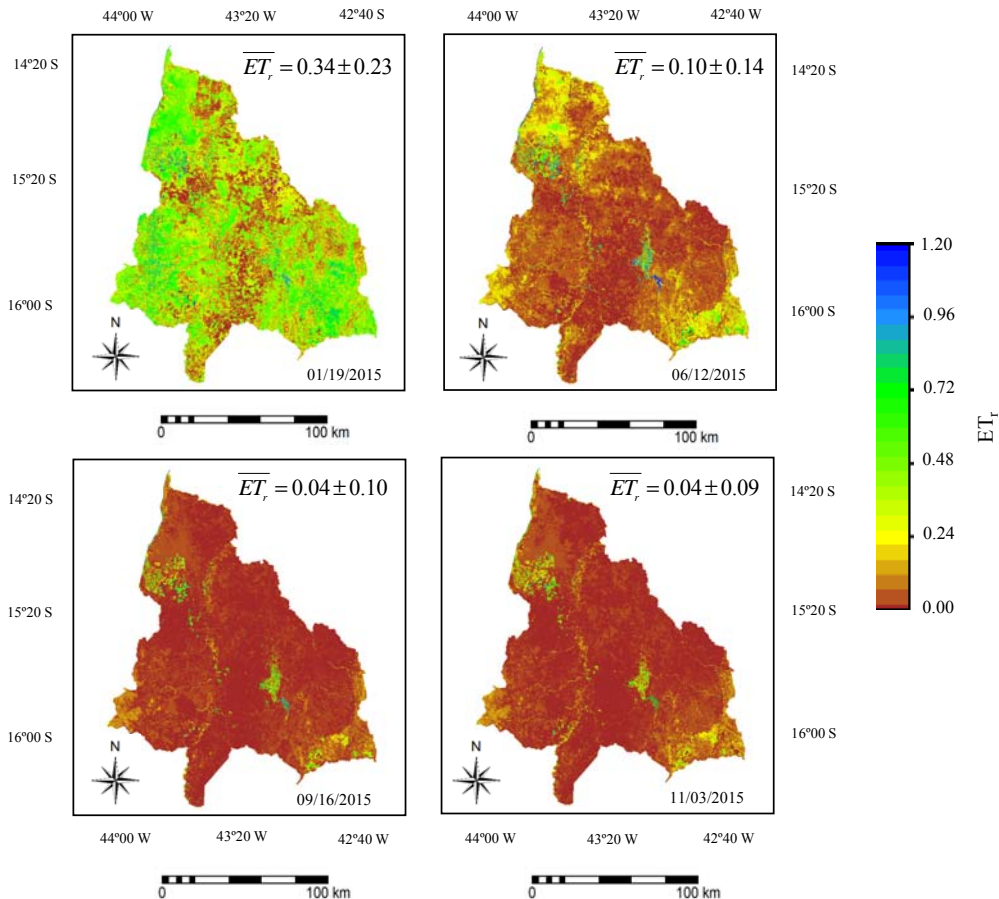


**Fig. 4** Spatial distribution and daily average values of the evapotranspiration ratio ( $ET_r$ ) index for different thermohydrological conditions during the year 2015, in the North of Minas Gerais state, Southeast Brazil. Overbars mean average values, shown together with the standard deviations.

The  $ET_r$  spatial variations in the mixed agro-ecosystems along the year 2015 are very clear, confirming the SAFER sensibility to monitor drought events under semi-arid conditions. Moisture pixel distinctions are most strongly noticed when comparing

the rainy period of the year 2015, from January 19 (DOY 019), when the  $ET_r$  values were above 0.90 in large part of the study region, with those which reflect the driest conditions in November 03, when some pixel values dropped  $ET_r$  to 0.00 (see Figs. 3 and 4). During

this last period, well-irrigated crops of the IC ecosystem presented  $ET_r$  values above 0.90.

The highest  $ET_r$  values in Jaíba, Nova Porteirinha and Riacho dos Machados counties, during the climatically driest periods (see Figs. 1 and 4), may be attributed to the largest concentrations of irrigation areas.

Zhang et al. [13] reported  $ET_r$  values for vegetation in deserts under the temperate climate environments, in Mongolia, China, with values ranging from 0.16 to 0.75, similar to several conditions of the current study. However, Lu et al. [6], in the same Chinese region, found  $ET_r$  values above 1.00 for six different ecosystems. Zhou and Zhou [14] concluded that air

temperature and air humidity as well as the available energy are the most important issues for the  $ET_r$  spatial variations.

In the North of Minas Gerais state, Southeast Brazil, the most important weather driver for increasing  $ET_r$  was the rainfalls happening previously to the image acquisition dates, which contributed to increments on soil moisture in the subsequent periods.

Fig. 5 shows the spatial distribution of the index surface resistance to water fluxes ( $r_s$ ) values for periods with different thermohydrological conditions during the year 2015, in the Minas Gerais state, Southeast Brazil.

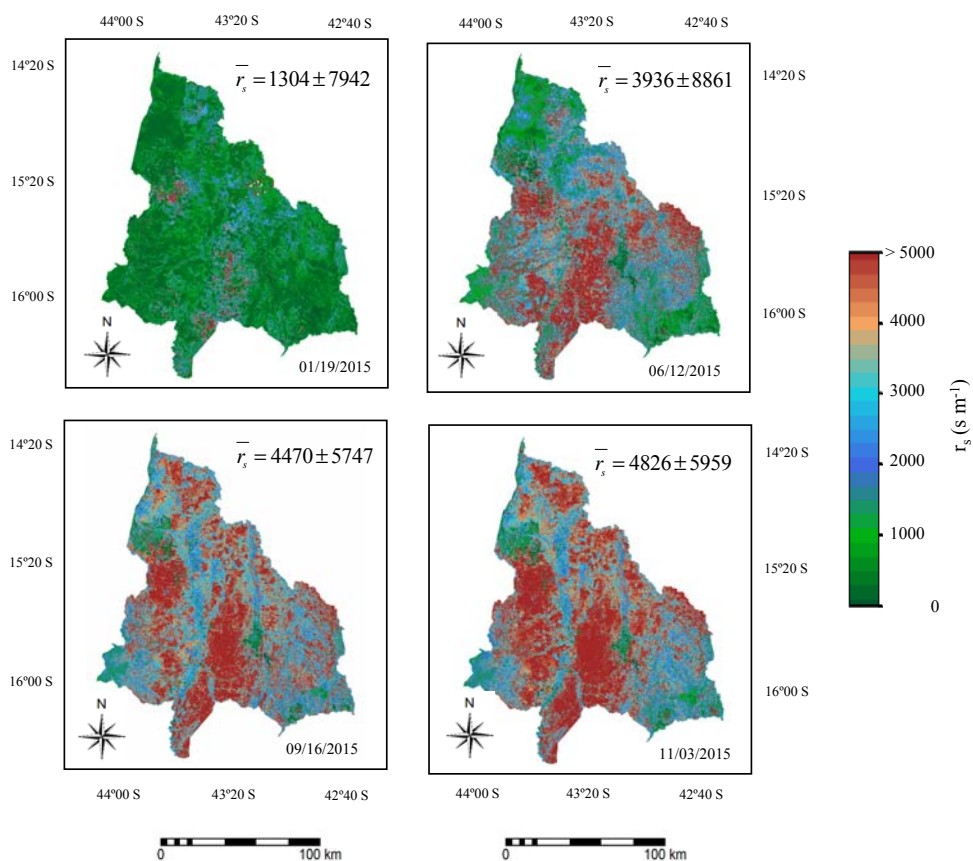


**Fig. 5** Spatial distribution and average pixel values for the surface resistance to water fluxes ( $r_s$ ), under different thermohydrological conditions of the year 2015, in the North of Minas Gerais state, Southeast Brazil. The overbars mean average pixel values, shown together with the standard deviations.

Pixels with  $r_s$  values lower than  $800 \text{ s m}^{-1}$  and NDVI above or equal to 0.30 were classified as irrigated crops (IC). When the  $r_s$  values were in between  $1,000$  and  $10,000 \text{ s m}^{-1}$ , the ecosystems were classified as natural

vegetation (NV). The high end of this range was considered to exclude human buildings and rocks [7, 8].

The lowest  $r_s$  values translated well root-zone moisture conditions, while the highest ones may be related to dryness conditions. The spatial and temporal variations are also very clear, bringing additional confidence to the SUREAL algorithm for detecting water and vegetation different conditions on large scales.

However, comparing the images of September 16 and November 03, acquired during the driest conditions of the year 2015 in Figs. 4 and 5, it is strongly noticed that  $r_s$  translate better the root-zone moisture than  $ET_r$ , by a better stratification of the pixels. The strong relation of  $r_s$  with the water and vegetation conditions in the current study confirm the suitability of this index to monitor dry spells for specific years on large scales in semi-arid environments [7].

Besides  $ET_r$  being a root-zone moisture index, when multiplied by the  $ET_0$  grids, retrieves the large-scale ET values throughout the SAFER application. With the SUREAL algorithm, we could retrieve specific ET pixel values for IC and NV agro-ecosystems.

Fig. 6 presents the average values and standard deviations of ET for the IC and NV agro-ecosystems in the semi-arid region of the North of Minas Gerais state, Southeast Brazil, in terms of day of the year (DOY).

For both agro-ecosystems, IC and NV, the highest ET rates were in January, conditions represented by the image of image of DOY 019. During this period, taking the high end of the standard deviations, because of the coupled water supply from rains and irrigation, IC reached to a maximum of  $4.7 \text{ mm d}^{-1}$ , representing the well-irrigated crops, while the maximum one for the NV ecosystem was  $2.7 \text{ mm d}^{-1}$ , resulted from the increase in the root-zone moisture by the previous precipitations.

Along the year, however, ET from the NV ecosystem was progressively declining to average values close to zero in November (DOY 307), in the IC another high average value of  $3.1 \pm 1.2 \text{ mm d}^{-1}$  happened. This extra water consumption generated an incremental value of  $3.0 \text{ mm d}^{-1}$ , because of the replacement of the “Caatinga” species by agriculture.

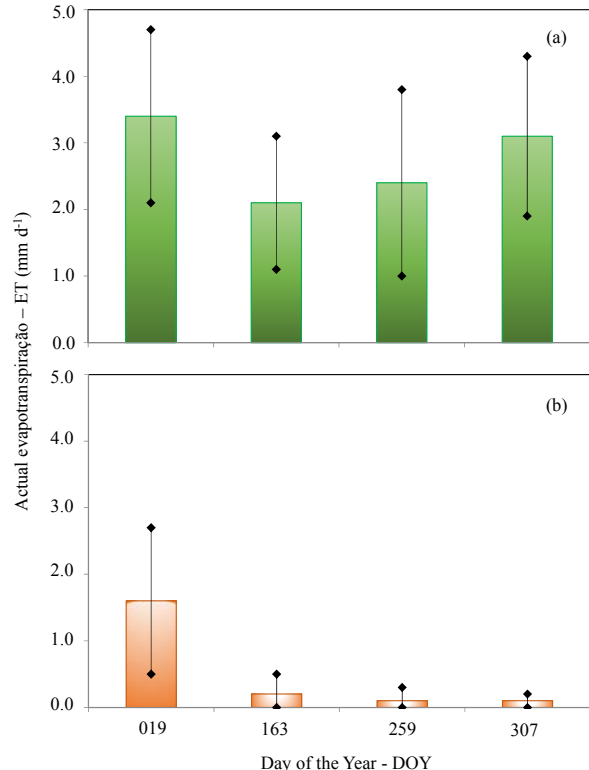


**Fig. 6** Average values and standard deviations for daily actual evapotranspiration (ET) in different agro-ecosystems of the North of Minas Gerais state, Southeast Brazil, in terms of day of the year (DOY): (a) Irrigated crops – IC and (b) natural vegetation – NV.

Leivas et al. [15] reported top ET values of  $3.5 \pm 1.0 \text{ mm d}^{-1}$  in irrigation pivots by using MODIS images in Jaíba County in the North of Minas Gerais, Southeast Brazil. The similarity between their values with those of the current study brings extra confidence to the SUREAL applications in semi-arid regions.

#### 4. Conclusion

The use of Landsat 8 images and net of agrometeorological stations for large-scale modelling water and vegetation indices in semi-arid regions is very suitable. It was demonstrated that the coupled use of the SAFER and SUREAL can retrieve specific values of these indices irrigated crops and natural vegetation, detecting the extra water consumption resulted from the replacement of natural species by agriculture. The results are relevant for monitoring drought events under the additional environmental

consequences of land use change in semi-arid environments.

## References

- [1] World Meteorological Organization (WMO) and Global Water Partnership (GWP), Drought Management Programme (IDMP), Integrated Drought Management Tools and Guidelines Series 2. Geneva, 2016.
- [2] A. H. de C. Teixeira, Modelling water productivity components in the Low-Middle São Francisco River basin, Brazil, in: C. Bilibio, O. Hensel (Eds.), J. Selbach (Org.), *Kassel Sustainable Water Management in the Tropics and Subtropics and Case Studies in Brazil*, University of Kassel, 2012a.
- [3] X. Cai, C. Mckinney and S. Lasdon, A framework for sustainable analysis in water resources management and application to the Syr Darya Basin, *Water Resources Research* 38 (2002) 21-24.
- [4] A. H. de C. Teixeira, J. F. Leivas, R. G. Andrade, D. de C. Victoria, E. L. Bolfe and G. B. Silva, Water balance indicators from MODIS images and agrometeorological data in Minas Gerais state, Brazil, *Proceedings of SPIE* 9637 (2015) 96370O-1-96370O-14.
- [5] R. G. Allen, L. S. Pereira, D. Raes, D., M. Smith, Crop evapotranspiration, Guidelines for computing crop water requirements, FAO Irrigation and Drainage Paper 56, 1998, p. 300.
- [6] N. Lu, S. Chen, B. Wilske, G. Sun, J. Chen, Evapotranspiration and soil water relationships in a range of disturbed and undisturbed ecosystems in the semi-arid Inner Mongolia, China, *Journal of Plant Ecology* 4 (2011) 49-60.
- [7] A. H. de C. Teixeira, Determination of surface resistance to evapotranspiration by remote sensing parameters, in the semi-arid region of Brazil for land-use change analyses, in: Neale C. M. U., Cosh, M. H., *Remote Sensing and Hydrology* (157th ed.), Vol. 352, Wallingford, UK: IAHS Press, 2012b, pp. 167-170.
- [8] J. F. Lumbreras, U. J. Naime, A. P. de Oliveira, L. F. Silva Neto da, A. de Carvalho Filho, P. E. F. da Motta, S. B. Calderano, M. L. R. Simão, M. L. D. Áglio, E. M. Vieira, M. L. Machado, A. J. R. dos Santos, D. C. da Silva, J. S. de Souza, A. R. Ferreira, Levantamento semi detalhado dos solos do Projeto Jaíba (Etapa III), Estado de Minas Gerais. Dados eletrônicos, Rio de Janeiro, Embrapa Solos, 2014, p. 148 (Boletim de pesquisa e desenvolvimento No. 248 /Embrapa Solos).
- [9] A. H. de C. Teixeira, Determining regional actual evapotranspiration of irrigated and natural vegetation in the São Francisco river basin (Brazil) using remote sensing and Penman-Monteith equation, *Remote Sensing* 2 (2010) 1287-1319.
- [10] A. H. de C. Teixeira, J. F. Leivas, F. B. T. Hernandez, R. A. M. Franco, Large-scale radiation and energy balances with Landsat 8 images and agrometeorological data in the Brazilian semiarid region, *Journal of Applied Remote Sensing* 11 (2017) 016030.
- [11] Q. Vanhellemont and K. Ruddick, Turbid wakes associated with offshore wind turbines observed with Landsat 8, *Remote Sensing of Environment* 145 (2014), 105-115.
- [12] M. R. Raupasch, Combination theory and equilibrium evaporation, *Quarterly Journal of the Royal Meteorological Society* 127 (2001) 1149-1181.
- [13] F. Zhang, G. Zhou, Y. Wang, F. Yan, C. Christer Nilsson, Evapotranspiration and crop coefficient for a temperate desert steppe ecosystem using eddy covariance in Inner Mongolia, China, *Hydrological Processes* 26 (2012) 379-386.
- [14] L. Zhou and G. Zhou, Measurement and modeling of evapotranspiration over a reed (*Phragmitesaustralis*) marsh in Northeast China, *Journal of Hydrology* 372 (2009) 41-47.
- [15] J. F. Leivas, A. H. de C. Teixeira, G. B. Silva, C.C. Ronquim and J. B. R. S. Reis, Biophysical indicators based on satellite images in an irrigated area at the São Francisco River, *Proceedings of SPIE* 9998 (2016) 99981N-1-99981N-9.